CHAPTER 5

Bifurcations in a two-block stick-slip system

"The most exciting phrase to hear in science, the one that heralds new discoveries, is not Eureka! but That's funny ... ".

Isaac Asimov (1920-1992)

In this chapter the dynamic behaviour of the two-block Burridge-Knopoff model for earthquake simulations is investigated. Previous numerical studies investigated in [113] verified that, with a friction force of Coulomb type (that is the dynamic friction coefficient being constant), the system presents only periodic behaviour. We will show that chaotic regions can be observed in a symmetric configuration even if a Coulomb friction is considered with the relaxation of the assumption that the driving block does not move during the slipping events. Furthermore, we will study the behaviour of the system with asymmetric configuration. Different periodic solutions and regions of chaos can be observed varying the asymmetry of the system. With respect to the bifurcation point of view, this system can exhibit smooth and discontinuity-induced bifurcations as we will present in this chapter.

5.1 Introduction

Along the Earth's plate boundaries, such as the San Andreas fault (see Fig. 5.1), segments exist where no large earthquakes have occurred for long intervals of time. Scientists term these segments "seismic gaps" and, in general, have been successful in forecasting the time when some of the

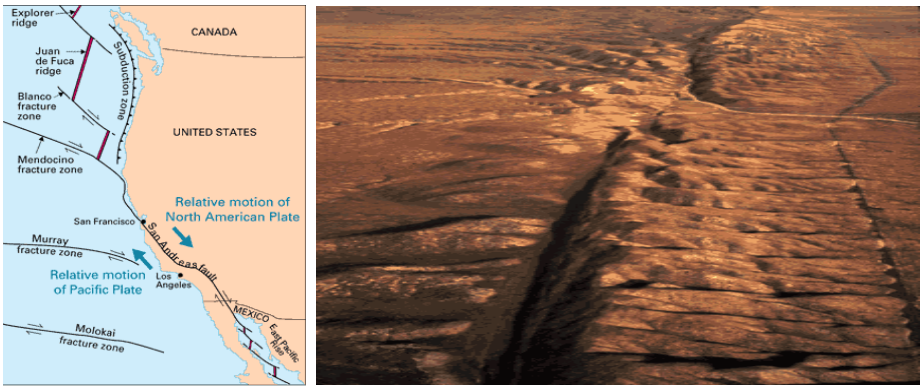

Figure 5.1: San Andreas fault

seismic gaps will produce large earthquakes. Geologic studies show that over the past 1500 years large earthquakes have occurred at about 150-year intervals on the southern San Andreas fault. As the last large earthquake on the southern San Andreas occurred in 1857, that section of the fault is considered a likely location for an earthquake within the next few decades.

Therefore, deterministic models of earthquake faults are important for understanding the mechanism for their observed behaviour in nature, such as Gutenberg-Richter scaling. These models are used with the hope of simulating seismic patterns, and observing such features as a reasonable frequency-magnitude relationship. To address the spatial aspect of seismicity patterns, Burridge and Knopoff [26] (1967) studied (experimentally and numerically) a one-dimensional chain of blocks connected by springs. Since this work, several papers have investigated the behaviour of the Burridge-Knopoff model for earthquakes using similar models, different friction laws, elastic properties, initial states, and loading conditions.

The occurrence of an earthquake involves the formation of a pressure bond between adjacent crustal blocks, which allows for a build up of elastic strain potential energy. Once the potential energy exceeds the strength of the pressure bond, brittle fracture occurs to release the strain, and the potential energy is converted into kinetic energy. When a slider-block system to model faults is used, it is usually assumed that each block represents a segment of a fault and the system can be considered analog to an interacting system of faults. Then, the extension of the springs is analogous to the elastic strain in the rock adjacent to a fault and the slip is analogous to an earthquake on a fault.

In this chapter we have simulated a two-block mass-spring model with static/dynamic friction. The papers concerned with the seismological interpretation of the model focus mainly on chaotic attractors, the only attractors that are of relevance to seismology. With respect to the chaotic properties of the model, we are aware of the numerical studies performed by Nussbaum and Ruina [113], Huang and Turcotte [85], Lacorata and Paladin [119], and Sousa [134] using different assumptions. In [113] the following assumptions are considered:

1. The driver is assumed to move slowly, so slowly that it may be considered stationary during any block motion (as in [26]). Therefore, the driving block does not move during the slipping events.

2. A symmetric model is considered ($\beta = 1$). Therefore, the friction forces in both blocks are the same.

3. A Coulomb friction force is assumed, i.e., static/dynamic friction forces are considered constants.

4. Slip occurs in only one direction (block velocities are never positive during slip), *i.e.*, back-slip is prevented.

Under these assumptions, it was verified in [113] that the system presents only periodic behaviour. In [85] a chaotic behaviour was found with the presence of an asymmetry in the system but considering a velocity weakening friction force. In particular, [85] considered the friction force in one block to be different from the friction force in the other block. Using the same friction law, Lacorata and Paladin [119] showed also a chaotic behaviour in an asymmetric model but with assumption 1 rejected. Furthermore, Sousa [134] showed that the two-block Burridge-Knopoff model given in [85] in a symmetric configuration is also chaotic but also rejecting the assumption 1. However, there is no evidence of chaos using a Coulomb friction force law, as in [113], in the symmetric model. In this chapter, we will show that the symmetric configuration has also chaotic regions if assumption 1 is not considered.

Galvanetto [76] highlighted the possible consequences of considering the assumption of symmetry (assumption 2) frequently made in the papers that are more seismologically oriented. In particular, in his opinion asymmetric systems are preferable in order to simulate more closely the real behaviour of earthquake faults. Therefore, in this work we will present the different solutions varying the asymmetry parameter in the model used

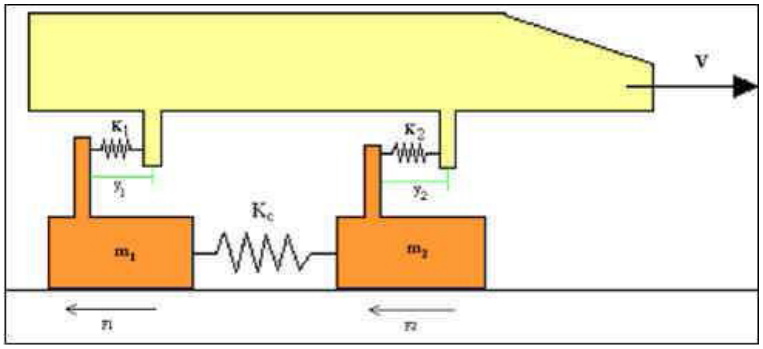

Figure 5.2: Illustration of the two blocks model with a constant velocity driver.

by [113]. Indeed, we have simulated a "brute-force" two-dimensional bifurcation diagram in order to see the different attractors.

As it is outlined also in [76], chaotic attractors are not the only attractors of Burridge-Knopoff systems but in seismological literature there is almost no mention of periodic and quasi-periodic attractors. Indeed, the two-block stick-slip system is an interesting example of nonsmooth system and therefore it should be better investigated from a bifurcation point of view. In [71, 72, 74, 75], disregarding assumptions 1,2 and 4, different smooth and nonsmooth bifurcations have been produced. In this chapter, we will show that discontinuity-induced bifurcations (DIBs) are also possible considering the model used in [113].

After describing the mechanical model in section 5.2, we will describe the different analytical solutions depending on the state of each mass and whether assumption 1 is considered or not. In section 5.4 a one-dimensional map, which characterizes the system, is presented. In section 5.5 we will show that chaotic regions can be present in a symmetric configuration if we allow the driving block to move during the slipping events. A two-dimension bifurcation diagram will be depicted in section 5.6 in order to show the different behaviours exhibited when the asymmetry parameter is varied. Furthermore, some smooth and sliding bifurcations are explained in section 5.7. Finally, we summarize our conclusions in section 5.8.

5.2 The Mechanical Model

The nonsmooth mechanical model usually presented in the papers that are more seismologically oriented is illustrated in Fig. 5.2. Such model considers of two blocks of masses $\mathbf{m}_1$ and $\mathbf{m}_2$ attached to each other by a spring with constant $\mathbf{k}_c$ and attached to a constant velocity driver with velocity $\mathbf{v}$, by springs with constants $\mathbf{k}_1$ and $\mathbf{k}_2$. The position coordinates for each block, referred to the constant velocity driver, are $\mathbf{y}_1$ and $\mathbf{y}_2$. The surface between the blocks and the belt is rough and it exerts a dry friction force on each block so that they stick to the surface until the point where the elastic forces due to the springs exceed the maximum static force. At this point the block starts slipping and the slipping motion will continue to the point were the velocity of the block will be equal to that of the driver and the elastic forces will be equilibrated by the static friction force. In this chapter no back-slip is considered and the dynamic of the system is described in what follows.

During a stick phase the displacement of a block is given as a function of time:

$$y_i(t) = y_i(t_0) + v \cdot (t - t_0), \qquad i = 1, 2 \tag{5.1}$$

where $y_i(t_0)$ is the initial displacement. The blocks can stick only if the following relations are true:

$$k_1 y_1 + k_c(y_1 - y_2) < f_{s1}, \tag{5.2}$$

$$k_2 y_2 + k_c(y_2 - y_1) < f_{s2}, \tag{5.3}$$

where f_{si} is the maximum static friction force acting on block i. The stick phase will end when one of the following conditions

$$k_1 y_1 + k_c(y_1 - y_2) = f_{s1}, \tag{5.4}$$

$$k_2 y_2 + k_c(y_2 - y_1) = f_{s2} \tag{5.5}$$

is satisfied. If the first condition is verified then block 1 will start slipping, whereas the second condition indicates the impending slip condition for the block 2. At one of these points a slip phase will begin according to the following equations of motion:

$$m_1 \ddot{y}_1(t) + k_1 y_1(t) + k_c(y_1(t) - y_2(t)) = f_{k1}(\dot{y}_1 - v), \tag{5.6}$$

$$m_2 \ddot{y}_2(t) + k_2 y_2(t) + k_c(y_2(t) - y_1(t)) = f_{k2}(\dot{y}_2 - v), \tag{5.7}$$

where $f_{ki}(\dot{x}_i - v)$ is the kinetic friction force, which is a function of the relative velocity of the block with respect to the driver. In general, the two blocks are not slipping at the same time and therefore there will be intervals of time in which the motion of one block is described by equation (5.1) and the motion of the other by equation (5.6) or (5.7). For that reason the phase space dimension of the system may be 2 if both blocks are stopped, 3 when one block is slipping and the other is sticking, and 4 when both blocks are slipping.

In order to simplify the model further, we assume that $m_1 = m_2 = m$, and $k_1 = k_2 = k$. Let us consider the dimensionless form of the above system given by the following equations:

Slip phases:

$$\ddot{Y}_1(\tau) + Y_1(\tau) + \alpha(Y_1(\tau) - Y_2(\tau)) = F_{k1}(\dot{Y}_1 - V_{dr}), \tag{5.8}$$

$$\ddot{Y}_2(\tau) + Y_2(\tau) + \alpha(Y_2(\tau) - Y_1(\tau)) = F_{k2}(\dot{Y}_2 - V_{dr}), \tag{5.9}$$

Slipping conditions:

$$Y_1 + \alpha(Y_1 - Y_2) = 1 \quad \text{(block one)}, \tag{5.10}$$

$$Y_2 + \alpha(Y_2 - Y_1) = \beta \quad \text{(block two)}, \tag{5.11}$$

Stick phase:

$$Y_i(\tau) = Y_i(\tau_0) + V_{dr}(\tau - \tau_0), \quad i = 1, 2. \tag{5.12}$$

where $\beta = \frac{f_{s2}}{f_{s1}}$, $\alpha = \frac{k_c}{k}$, $Y_i = \frac{k y_i}{f_{s1}}$, $\tau = \sqrt{\frac{k}{mt}}$, $V_{dr} = \frac{v\sqrt{km}}{f_{s1}}$. Notice that the system is symmetric if $\beta = 1$.

Inequalities $Y_1 + \alpha(Y_1 - Y_2) < 1$ and $Y_2 + \alpha(Y_2 - Y_1) < \beta$ define an open convex region in the space of the displacement variables (Y_1, Y_2) as shown in Fig. 5.3. Such region is the locus where both blocks are simultaneously sticking and will be called the global stick phase locus.

The friction force characteristic may assume different forms, the most common of which is the Coulomb friction that, in dimensionless terms, is given by the following expression:

$$F_k(\dot{Y} - V_{dr}) = \begin{cases} 1 & \text{if } V_{dr} - \dot{Y} = 0 \\ \mu_k & \text{if } V_{dr} - \dot{Y} > 0 \end{cases} \tag{5.13}$$

where $0 < \mu_k < 1$ is a constant and therefore the kinetic friction is a constant force opposing the relative motion between block and driver, smaller

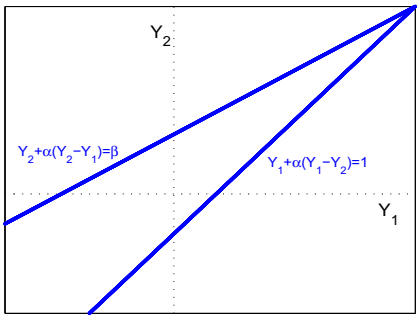

Figure 5.3: The open convex region of the plane limited by the blue lines is the global stick phase locus of the system.

in magnitude than the maximum static friction force F_s ($F_s = 1$ in dimensionless terms). Note that for our system $\mu_{k2} = \beta\mu_{k1}$.

Another commonly used friction characteristic [85, 134, 32] is given by the velocity weakening friction force:

$$F_k(\dot{Y} - V_{dr}) = \frac{1}{1 + |\dot{Y} - V_{dr}|} \tag{5.14}$$

In this chapter we will use the Coulomb friction characteristic in order to show that using this friction law it is possible to find different complex behaviours as well of those that have been reported in the literature with a velocity weaking friction force.

5.3 Dynamics of the model

The dynamics of the model can be splitted in four different states depending on which block is slipping. In this section, we will give the analytical solution of each state with and without considering the assumption 1 given in 5.1. Let us denote $\phi = \frac{1}{\mu_k}$ in what follows. Then, we can consider the following states:

- STATE 1: This state is when both masses are stopped. Then the system is ruled by the analytical solutions given in (5.12). As both masses are stopped the system will remain in this state until one of them begin its movement, *i.e.*, until condition (5.10) or (5.11) hold.

- STATE 2: This state appears when the second block is slipping while the first one is stopped. The system is determined by the following analytical solution:

$$Y_1(\tau) = Y_{10} + V_{dr} \cdot \tau, \tag{5.15}$$

$$Y_2(\tau) = \frac{\alpha(Y_{10} + V_{dr}\tau) + \beta\mu_k}{(1+\alpha)} + \frac{(\dot{Y}_{20} - \frac{\alpha V_{dr}}{1+\alpha})\sin((\sqrt{1+\alpha}) \cdot \tau)}{\sqrt{1+\alpha}} - \\ - \frac{(\alpha Y_{10} + \beta\mu_k - Y_{20}(1+\alpha))\cos((\sqrt{1+\alpha}) \cdot \tau)}{1+\alpha} \tag{5.16}$$

where $Y_{10} = Y_1(t_0)$, $Y_{20} = Y_2(t_0)$, and $\dot{Y}_{20} = \dot{Y}_2(t_0)$ are the initial conditions in this state. In this case, the change of state happens if the first mass starts to move or the second one stops. Therefore in this state, the conditions for the change of state are:

$$Y_1(\tau) + \alpha(Y_1(\tau) - Y_2(\tau)) = 1 \tag{5.17}$$

$$\frac{dY_2}{d\tau}(\tau) = V_{dr} \tag{5.18}$$

If the first equation is satisfied, the first block will start to move, and if the second equation is satisfied, the second mass will stop (therefore we change to the state 1).

Note that $V_{dr} = 0$ in equations (5.15), (5.16) and (5.18) of this state if the assumption 1, introduced in section 5.1, is considered.

- STATE 3: This state correspond to both masses slipping. The system is ruled by these analytical solutions:

$$Y_1(\tau) = \frac{1+\alpha(1+\beta)}{\phi(1+2\alpha)} + \frac{1}{2\phi} \cdot \Big[\big((\dot{Y}_{10} + \dot{Y}_{20}) \cdot \phi \cdot \sin(\tau)\big) + \\ + \big(-(1+\beta) + (Y_{10} + Y_{20}) \cdot \phi\big) \cdot \cos(\tau) + \\ + \frac{(\dot{Y}_{10} + \dot{Y}_{20}) \cdot \phi \cdot \sin(\sqrt{1+2\alpha} \cdot \tau)}{\sqrt{1+2\alpha}} + \\ + \frac{\big(\beta - 1 + (1+2\alpha) \cdot \phi \cdot (Y_{10} - Y_{20})\big) \cdot \cos(\sqrt{1+2\alpha} \cdot \tau)}{1+2\alpha}\Big] \tag{5.19}$$

$$Y_2(\tau) = \frac{\beta + \alpha(1+\beta)}{\phi(1+2\alpha)} + \frac{1}{2\phi} \cdot \Big[\big((\dot{Y}_{10} + \dot{Y}_{20}) \cdot \phi \cdot \sin(\tau) \big) + \\ + \big(-(1+\beta) + (Y_{10} + Y_{20}) \cdot \phi \big) \cdot \cos(\tau) - \\ - \frac{(\dot{Y}_{10} + \dot{Y}_{20}) \cdot \phi \cdot \sin(\sqrt{1+2\alpha} \cdot \tau)}{\sqrt{1+2\alpha}} - \\ - \frac{\big(\beta - 1 + (1+2\alpha) \cdot \phi \cdot (Y_{10} - Y_{20}) \big) \cdot \cos(\sqrt{1+2\alpha} \cdot \tau)}{1+2\alpha} \Big] \tag{5.20}$$

where $Y_{10} = Y_1(t_0)$, $Y_{20} = Y_2(t_0)$, $\dot{Y}_{10} = \dot{Y}_1(t_0)$, and $\dot{Y}_{20} = \dot{Y}_2(t_0)$ are the initial conditions in this state. As both masses are slipping the system will remain in this state until one of them stops. The first mass stops when the equation:

$$\frac{dY_1}{d\tau}(\tau) = V_{dr} \tag{5.21}$$

holds. For the another block the condition is:

$$\frac{dY_2}{d\tau}(\tau) = V_{dr} \tag{5.22}$$

- STATE 4: The first block is slipping while the second one is stopped. The analytical solutions are given by

$$Y_1(\tau) = \frac{\alpha(Y_{20} + V_{dr}\tau) + \mu_k}{1+\alpha} + \frac{(\dot{Y}_{10} - \frac{\alpha V_{dr}}{1+\alpha}) \sin((\sqrt{1+\alpha}) \cdot \tau)}{\sqrt{1+\alpha}} - \\ - \frac{(\alpha Y_{20} + \mu_k - Y_{10}(1+\alpha)) \cos((\sqrt{1+\alpha}) \cdot \tau)}{1+\alpha} \tag{5.23}$$

$$Y_2(\tau) = Y_{20} + V_{dr} \cdot \tau \tag{5.24}$$

with the following initial conditions: $Y_{10} = Y_1(t_0)$, $Y_{20} = Y_2(t_0)$, and $\dot{Y}_{10} = \dot{Y}_1(t_0)$. In this case, the change of state happens if the second mass starts to move or the first one stops. Therefore in this state, the conditions for the change of state are:

$$\frac{dY_1}{d\tau}(\tau) = V_{dr} \tag{5.25}$$

$$Y_2(\tau) + \alpha(Y_2(\tau) - Y_1(\tau)) = \beta \tag{5.26}$$

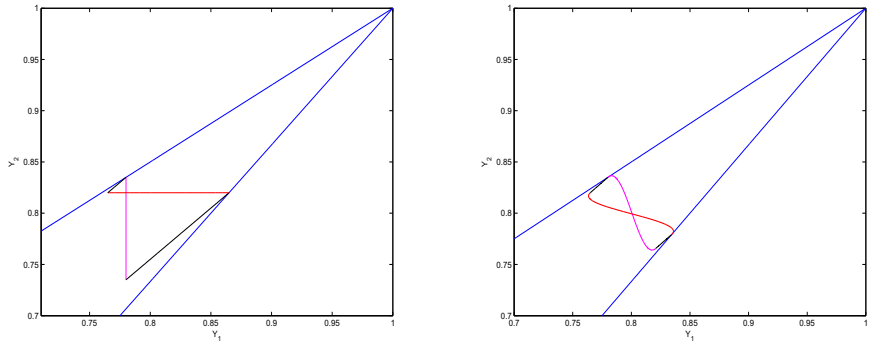

(a) (b)

Figure 5.4: Differences between considering or preventing assumption 1 ($\alpha = 3$, $\beta = 1$, $\phi = 1.25$ and $V_{dr} = 0.025$): (a) Periodic orbit considering assumption 1; (b) Period orbit being prevented assumption 1.

If the second equation is satisfied, the second block will start to move (therefore we change to state 3), and if the first equation is satisfied, the first mass will stop (therefore we change to the state 1).

Note that $V_{dr} = 0$ in the equations (5.23), (5.24) and (5.25) of this state if the assumption 1, introduced in section 5.1, is considered.

Notice that only during state 2 and 4 the assumption 1 has consequences. In Fig. 5.4 (a),(b) we have simulated a periodic orbit with and without considering assumption 1 under the same parameter values. As can be observed, the shape of the orbit is different in both cases, although the periodicity is the same. However, we will show later that structural changes can be also possible. States 1, 2 and 4 are depicted by black, pink and red lines respectively. In Fig. 5.4 (a) the assumption 1 is considered and both pink and red lines are straight because $V_{dr} = 0$ in the solution.

5.4 One-dimensional event map

The two-block stick-slip system can be studied using a one-dimensional map. The one-dimensional map was first introduced in the seismological field [113] and for that reason it is called the *event-map*, since each iteration

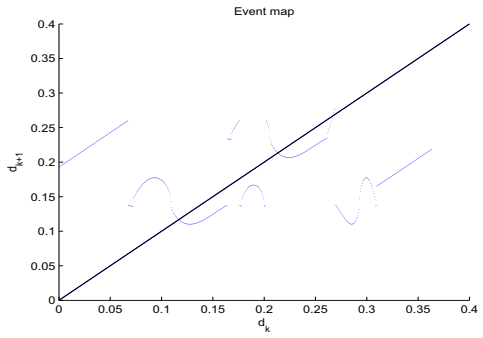

Figure 5.5: Illustration of the one-dimensional event map.

corresponds to a seismic event (earthquake) of the stick-slip model. As we have mentioned before the system has dimension 2 when both blocks are simultaneously sticking (state 1). Such phase of motion is usually called global stick phase whereas a slip phase is defined by the slipping of at least one block. During a global sticking phase (GSP) the relative displacement between the two blocks is fixed; therefore the GSP may be characterised by the constant value of a variable d:

$$d = Y_2 - Y_1$$

The GSP will finish when one of the two blocks starts slipping. If V_{dr} is sufficiently small [70, 74] the system will reach again the state 1 after a while. The new GSP, in general, will be characterised by a value of the relative displacement d different from the one assumed during the previous GSP In this way a motion of the system generates an infinite sequence of values of the variable $d = d_1, d_2, \ldots, d_m, \ldots$, which can be interpreted as a map expressing d_{k+1} as function of d_k:

$$d_{k+1} = f(d_k)$$

The map is well defined if a GSP is always followed by another GSP In some cases the steady state motion has no GSP and therefore cannot be represented by the 1-dim map, but these cases require driving velocities higher than those used the literature. Moreover, the map is single valued because a value of the variable d uniquely determines the initial conditions at which one of the blocks will start slipping (see figure 5.5).

A periodic motion of period m exists if there is a value $n \in \mathbb{N}$ where $d_{n+m} = d_n$. We denote such periodic orbit as *m-periodic orbit*. In a periodic

motion the map is also periodic, whereas if a motion is not periodic it will generate a non-periodic map. As can be observed, in Fig. 5.5 the event-map is discontinuous. Therefore, this one-dimensional map is used to describe nonsmooth bifurcations of the two-blocks model. We will show later that, in order to find nonsmooth bifurcations, it is specially interesting to study the cases in which the discontinuity points coincide with steady states of the map.

5.5 Chaos in a symmetric configuration

Using the event-map explained above we will show that chaotic solutions can be also found in the symmetric model introduced by [113] by just rejecting assumption 1. In Fig. 5.6 a bifurcation diagram for the event map, $(Y_2 - Y_1)$, is plotted taking V_{dr} as the bifurcation parameter. Having fixed an initial condition, successive 350 iterates of the event map are taken, and to avoid the transient dynamics only the last 100 values d_k are plotted. This process is repeated for every discrete value of the bifurcation parameter in the interval $V_{dr} \in [0.015, 0.025]$. We have considered the following parameter values: $\alpha = 2.9, \beta = 1, \phi = 1.25, d_0 = 0.02$.

For $V_{dr} = 0.025$, a stable 2-periodic orbit is initially found and continued until some value near 0.021. Then, a period-doubling bifurcation occurs, and the stability of the 2-periodic orbit is lost in favour of the 4-periodic orbit which appears at this value. Decreasing the bifurcation parameter V_{dr} a cascade of period-doublings is found until a chaotic zone is reached. After reaching such zone several jumps in the chaotic region occur for smaller values of V_{dr}. Finally, there is a jump from the chaotic region to a 2-periodic orbit.

We have thus shown that chaotic attractors are also possible in a symmetric configuration using a Coulomb friction force law if assumption 1 is not considered. However, as it is said in [76], the symmetric model appears to be unlikely from a physical point of view and earthquake dynamics could be probably better simulated by non-symmetric models. For this reason, in the following section we will study our system under an asymmetric configuration.

5.6 Observed behaviours in an asymmetric model

In order to study the behaviour of the system given by [113] in a asymmetric configuration we have computed two-dimensional bifurcation diagrams.

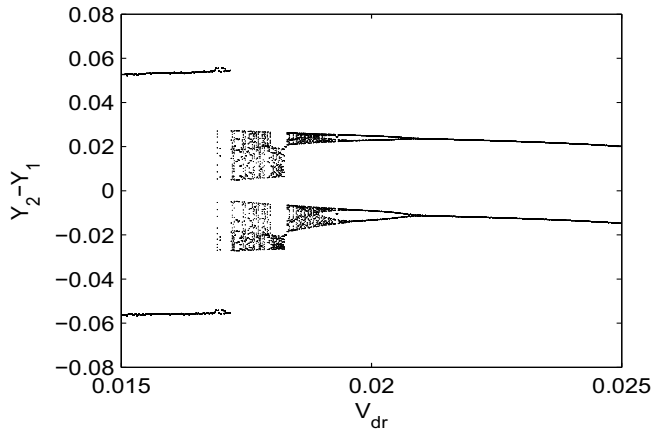

Figure 5.6: Bifurcation diagram

The bifurcation patterns will be obtained from different pairs of parameters. In particular, we have chosen (α, β) as varying parameters whereas the parameter ϕ will be constant ($\phi = 1.25$).

The two-dimensional bifurcation diagrams shown in this section are color-coded depending on the periodicity of the fixed points given by the event-map corresponding to the point in the parameter space. Due to the possibility of coexisting attractors, only one of them can be identified at each point of the parameter space. Indeed, the diagrams are produced as follows: first we give the extreme values of both varying parameters and an initial condition is fixed. In particular, we have taken the system starting in the state 1 and both initial positions equal to 0. Then, we compute the periodicity of the limit cycle obtained for each point in the parameter space. Finally, we assign a color depending on the periodicity. Notice that there can exist some parameter points with high periodicity and in order to simplify the diagram we plot chaos, quasiperiodicity and high periodicities (> 16) with the same color (see Fig. 5.7).

Notice that the periodicity of the limit cycle has been computed using the event map described in section 5.4. Therefore, we have considered as the period the number of times that the limit cycle is in different states 1. This implies that changes of periodicity can be due to smooth bifurcations or discontinuity-induced bifurcations such as sliding bifurcations (see chapter 4 for further details).

Using such numerical considerations we have calculated a two-dimensional

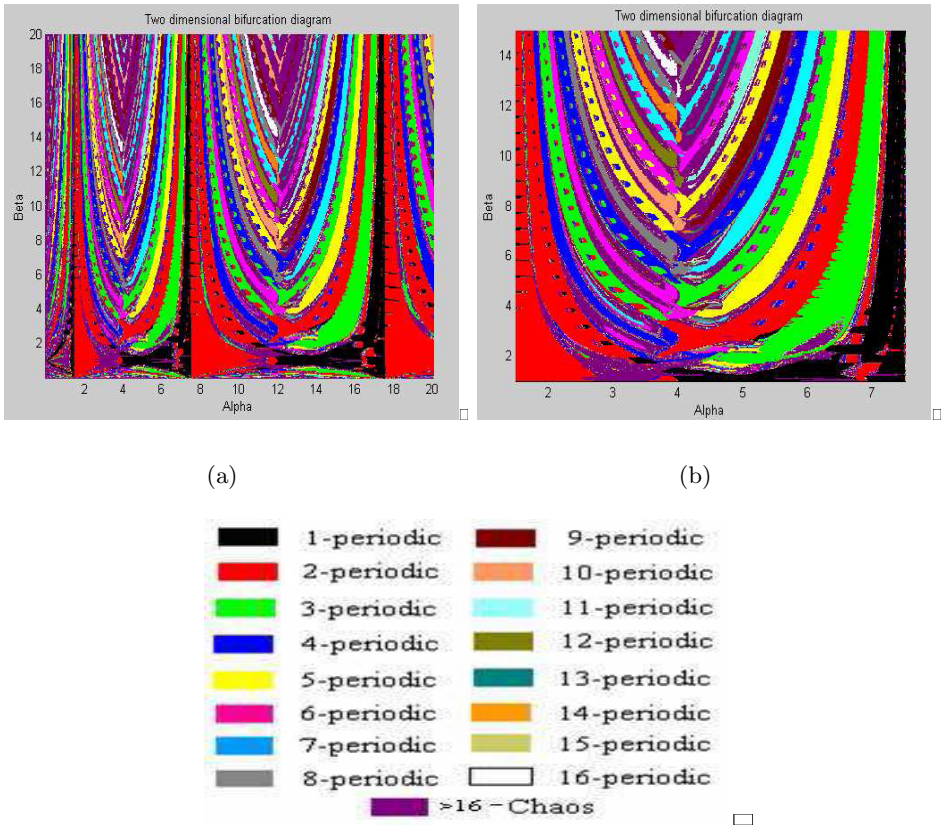

Figure 5.7: Two-dimensional bifurcation diagrams.

bifurcation diagram for the range $\alpha \in [1, 20]$ and $\beta \in [1, 20]$ (see Fig. 5.7 (a)). Two main characteristics can be observed in this figure. Firstly, we see that increasing β makes appear some regions with a higher periodicity. This gives us the idea that systems with a high asymmetry have more complexity. Secondly, we can distinguish a certain structure with respect to α. Between $\alpha = 1.5$ and $\alpha = 7.5$ there is a region of different behaviours that is repeated with a little vertical and horizontal expansion for higher values of α. This implies that all the information of this system is contained in this region (see Fig. 5.7 (b)). Moreover, inside of such region a pattern can be observed by varying β.

In Fig. 5.7 (b) a zoom of Fig. 5.7 (a) is depicted. It is also possible to see several windows inside of different regions of periodicity where there

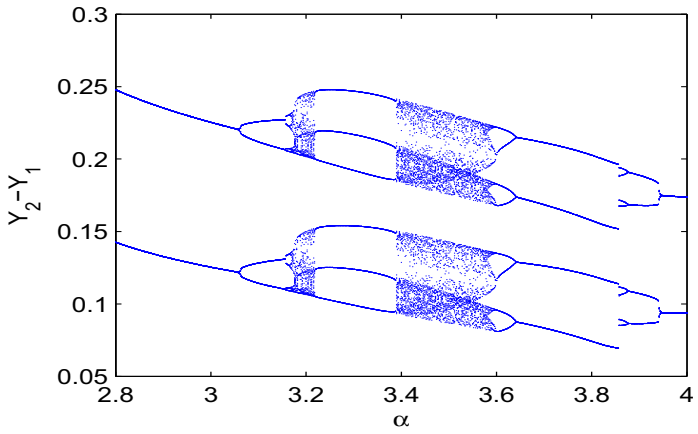

Figure 5.8: Bifurcation diagram

are coexisting solutions.

Although different one-dimensional bifurcation curves can be distinguished in both pictures, it is necessary to check in detail such regions in order to understand the bifurcation patterns better. In the next section we will describe some different bifurcation scenarios found in the asymmetric configuration.

5.7 Description of some bifurcations

As have been mentioned in section 5.1 the system under investigation can exhibit both smooth and discontinuity-induced bifurcations. In this section we will explain in detail some of the different observed behaviours presented in section 5.6. Four different bifurcation scenarios varying the parameter α will be studied. They are two smooth bifurcations, a flip and a fold bifurcation, and two sliding bifurcations, a crossing-sliding and a grazing-sliding bifurcation.

In Fig. 5.8 a one-parameter bifurcation diagram is depicted for the event-map. To calculate it we have used a brute-force method and the parameters assume the following values: $\beta = 2.5$ and $\phi = 1.25$, while α is varied in the range $[2.8, 4]$. For each value of α an initial condition is taken from the final state of the previous parameter value. Then, the system is simulated during a certain time (400 changes of state) and we plot the value of $Y_2 - Y_1$ during a GSP (state 1) for the last 150 changes of state.

As we have mentioned in previous chapters this method only finds stable solutions. In the next subsections will explain some different bifurcation scenarios that can be seen in such bifurcation diagram. Firstly, we will show two smooth bifurcations, a period doubling and a saddle-node bifurcation. Then, we will show two sliding bifurcations, namely a crossing-sliding and a grazing-sliding bifurcation.

5.7.1 Flip bifurcation

In the range $3 < \alpha < 3.2$ the system dynamics seem to undergo a period doubling cascade which is clearly described and confirmed by the use of the one-dimensional event-map. In Fig. 5.9 (a) the second iterated map is shown to have two stable attractors and an unstable fixed point. As the value of α increases, a period-doubling bifurcation occurs and the shape of the fourth iterated map changes in such a way that four stable attractors separated by two unstable points appear. Then, this periodic orbit loses stability in a period-doubling bifurcation for higher values of α and it follows a cascade of period-doublings until an apparently chaotic zone is reached.

5.7.2 Fold bifurcation

There is a fold bifurcation of the sixth iterated map for $\alpha \approx 3.215$ and $\alpha \approx 3.38$. Figure 5.10 (a) shows f^6 for $\alpha = 3.19$. For such value of α there is only an unstable fixed point out of the range shown in Fig. 5.10 (a). As we increase α the shape of the sixth iterated map changes and other six points of the map intersect with the bisection line for $\alpha \approx 3.215$. Then, a further increase of α gives six stable fixed points and six unstable fixed points (see Fig. 5.10 (b)) together with the unstable fixed point previously mentioned. Such stable and unstable period orbits disappear in another fold bifurcation for $\alpha \approx 3.38$. Indeed, if we decrease also the parameter β we find a codimension-two cusp bifurcation as in the previous chapter.

This system has also discontinuity-induced bifurcations such as sliding bifurcations. For $\alpha \approx 3.855$ there is a grazing-sliding bifurcation (see Fig. 5.8). In Fig. 5.11 (a)-(b) the event map for $\alpha = 3.85$ and $\alpha = 3.86$ is depicted. The stable periodic orbit disappears when α is increased, due to the discontinuity in the event-map. In what follows we will show another grazing-sliding bifurcation and therefore, we will not explain the present case in more detail.

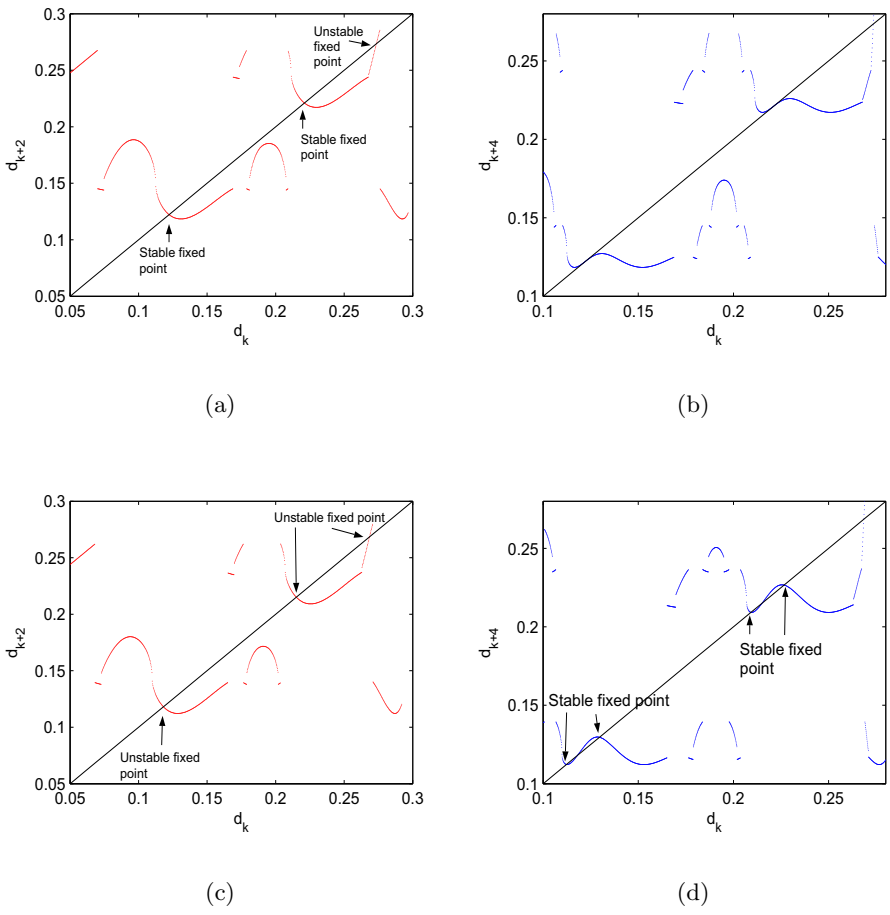

Figure 5.9: Flip bifurcation: (a) Second iterated map for $\alpha = 3.05$, (b) Fourth iterated map for $\alpha = 3.05$, (c) Second iterated map for $\alpha = 3.15$ and (d) Fourth iterated map for $\alpha = 3.15$.

In order to show two sliding bifurcations in detail we have calculated another one-dimensional bifurcation diagram for the event-map, see Fig. 5.12, considering the following parameters: $\beta = 3.2$ and $\phi = 1.25$, while α is varied in the range [5, 6.5]. We have also used the brute-force method but in this case we have varied α in both directions, *i.e.* we have firstly calculated the bifurcation diagram increasing the α parameter value from 5 to 6.5 and after that decreasing it from 6.5 to 5.

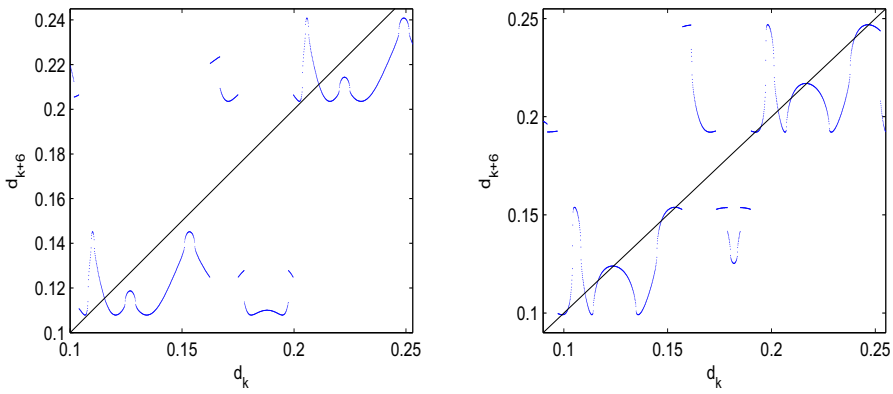

(a) (b)

Figure 5.10: Fold bifurcation: (a) Sixth iterated map for $\alpha = 3.19$ and (b) Sixth iterated map for $\alpha = 3.23$.

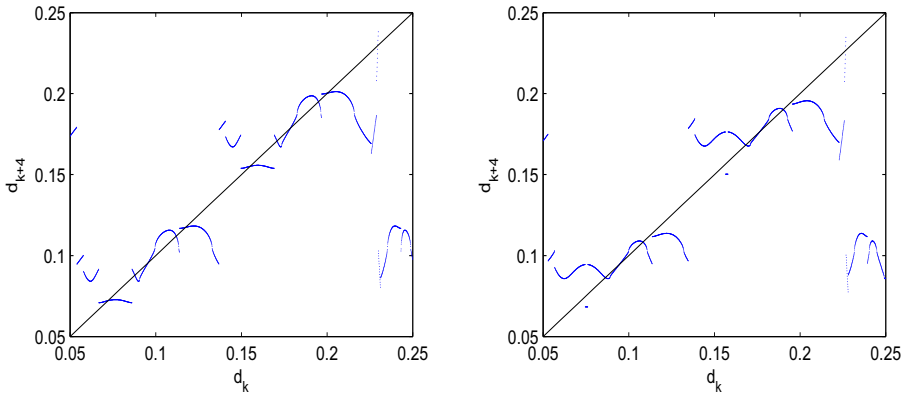

(a) (b)

Figure 5.11: Grazing-sliding bifurcation: (a) Fourth iterated map for $\alpha = 3.85$, and (b) Fourth iterated map for $\alpha = 3.86$.

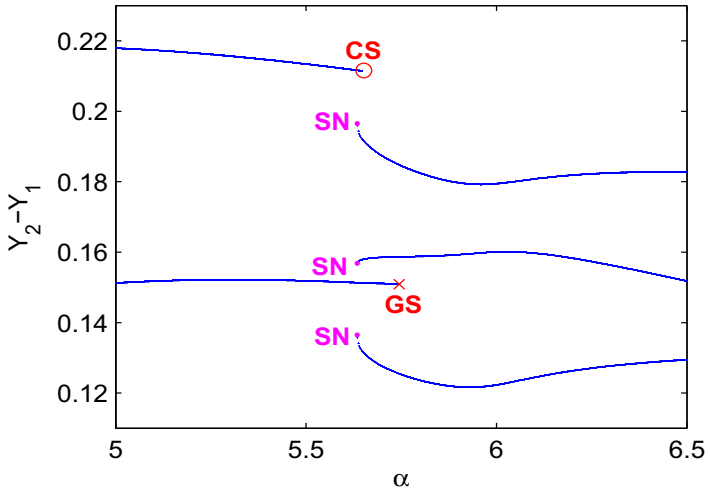

Figure 5.12: Bifurcation diagram

5.7.3 Crossing-sliding bifurcation

For $\alpha = 5$ there is a periodic orbit with two different GSP (a periodic motion of period 2 for the event-map). As we increase α the dynamical system undergoes to a crossing-sliding bifurcation. For $\alpha \approx 5.6$ one of the GSP disappears and therefore, the periodic motion for the event-map changes the periodicity. We can better observe such sliding bifurcation plotting the difference between the relative velocities of both masses (see Fig. 5.13). The periodic orbit intersects the boundary of the sliding region and one of the GSP is removed.

5.7.4 Grazing-sliding bifurcation

There is a coexistence of solutions for values of α between 5.6 and 5.7. We have the periodic orbit mentioned before and another period orbit with three different GSP. For $\alpha \approx 5.7$ the periodic orbit with one GSP undergoes a grazing-sliding bifurcation. Such bifurcation is due to the fact that the relative velocity of the mass 1 grazes the boundary of the sliding region (relative velocity equal to zero). In Figure 5.14 the evolution in time of the relative velocity of the mass 1 is depicted, just before that bifurcation occurs. For further increases of α the stable periodic orbit disappears, and

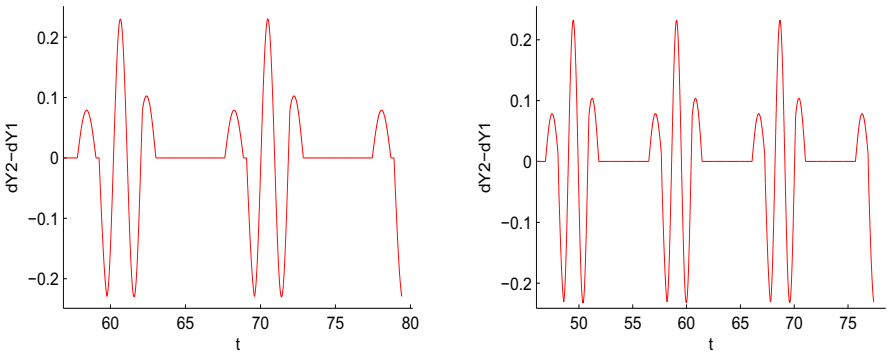

(a) (b)

Figure 5.13: Crossing-sliding bifurcation: Difference between the relative velocities of both masses (a) $\alpha = 5.58$, and (b) $\alpha = 5.62$.

therefore, the dynamics is governed by the other stable attractor. Notice also that the stable periodic orbit corresponding to the periodic orbit with period 3 in the event-map undergoes a fold bifurcation for $\alpha \approx 5.6$.

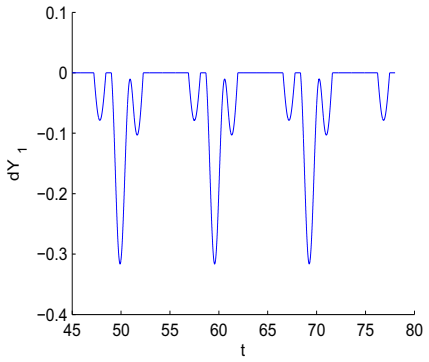

Figure 5.14: Grazing-sliding bifurcation: Relative velocities of mass 1 for $\alpha = 5.69$.

5.8 Conclusions

We have presented a numerical study of a two-block Burridge-Knopoff model considering the model introduced in [113]. A period-doubling cascade route to chaos has been found in a symmetric configuration and therefore, we have proved that chaotic regions can be observed even if a Coulomb friction is considered. A two-dimension bifurcation diagram gives an idea of the complexity of our system in an asymmetric configuration. Furthermore, analysing in more detail some regions we have found smooth and discontinuity-induced bifurcations. We have presented smooth bifurcations, a period-doubling and a saddle-node, and two sliding bifurcations, a crossing-sliding and a grazing-sliding.